Quantum emitters coupled to surface plasmons of a nanowire: A Green's function approach

David Dzsotjan,[1,2] Anders S. Sørensen,[3] and Michael Fleischhauer[1]
[1]*Department of Physics and Research Center OPTIMAS, University of Kaiserslautern, Kaiserslautern, Germany*
[2]*Research Institute for Particle and Nuclear Physics, H-1525 Budapest, Hungary*
[3]*QUANTOP, Danish National Research Foundation Center for Quantum Optics, Niels Bohr Institute, DK-2100 Copenhagen, Denmark*
(Received 16 February 2010; revised manuscript received 15 July 2010; published 27 August 2010)

We investigate a system consisting of a single, as well as two emitters strongly coupled to surface plasmon modes of a nanowire using a Green's function approach. Explicit expressions are derived for the spontaneous decay rate into the plasmon modes and for the atom-plasmon coupling as well as a plasmon-mediated atom-atom coupling. Phenomena due to the presence of losses in the metal are discussed. In case of two atoms, we observe Dicke subradiance and superradiance resulting from their plasmon-mediated interaction. Based on this phenomenon, we propose a scheme for a deterministic two-qubit quantum gate. We also discuss a possible realization of interesting many-body Hamiltonians, such as the spin-boson model, using strong emitter-plasmon coupling.

DOI: 10.1103/PhysRevB.82.075427 PACS number(s): 42.50.Nn, 78.67.Uh, 03.65.Yz

I. INTRODUCTION

A strong coupling between individual quantum emitters and photons is one of the key ingredients for photon-based quantum information processing. It is needed to achieve a reliable transfer of excitation between stationary and flying qubits and to realize quantum logic operations. Strong radiative coupling requires a tight confinement of the electromagnetic field. This can be achieved, e.g., when quantum emitters are coupled to surface plasmons of conducting nanowires as proposed in Refs. 1 and 2. Besides its simple structure, the atom-nanowire scheme guarantees an exceptionally strong field-emitter coupling. The original setup involves a single atom placed close to the surface of a metallic wire having subwavelength radius. In the present paper we analyze this scheme in detail by means of a Green's function approach taking into account metal losses and extend it to a plasmon-mediated coupling between different atoms. The unique properties of the propagating electromagnetic modes of the wire, the surface plasmons, have opened up new possibilities in many fields such as waveguiding below the diffraction limit,[3] subwavelength imaging,[4,5] or enhanced fluorescence.[6–10] The small transverse-mode area also enables one to strongly couple an emitter to the plasmon, giving rise to a substantial Purcell effect with a Purcell factor of 10^2 or larger. The system has been proposed as an efficient single-photon generator[1,2] as well as a single-photon transistor,[11] strong emitter-plasmon coupling has been experimentally shown using quantum dots,[12] single plasmons along the wire have been detected, using *N-V* centers as emitters[13] and the wave-particle duality of surface plasmons has been verified in experiment.[14]

We describe a system where a single, as well as two emitters interact with the surface plasmons of the wire in a fully quantum mechanical approach. Due to the strong coupling, the plasmons mediate an intensive long-range interaction between different emitters. As a result, we observe subradiance and superradiance in a two-atom system which can be efficiently controlled by adjusting the distance between the atoms. Based on this phenomenon, we propose a possible scheme for a deterministic quantum phase gate involving three-level λ atoms and classical 2π laser pulses.

The paper is organized as follows: in Sec. II we introduce the Green's tensor of the system as well as the structure and properties of the guided modes. We also discuss the coupling of a single emitter to the plasmons, and the total spontaneous decay rate and the decay rate into the plasmon modes are calculated. Section III deals with the long-range interaction of two emitters coupled to the plasmon modes. We show that certain states exhibit Dicke subradiance and superradiance which can be controlled by adjusting the distance between the emitters. We also present a scheme for a deterministic quantum phase gate based on the controllable superradiance phenomenon. Both in the case of a single emitter, as well as a pair of them, we discuss the effects of losses in the metal and their consequences. Finally, we discuss a possible extension of the level scheme of the emitters to realize interesting many-body Hamiltonians such as spin-boson model using the coupling to nanowires. Section IV contains a summary of the results.

II. GREEN'S FUNCTION APPROACH AND GUIDED MODES OF THE WIRE

A. General framework

The aim of this work is to describe a two-level atom with an electric dipole transition of strength $\vec{d}$, which is coupled to the guided plasmon waves on a conducting nanowire. The atom interacts with the nanowire via the quantized electromagnetic field $\hat{\vec{E}}(\vec{r}_A)$ at the position of the atom. The interaction Hamiltonian in the dipole and rotating wave approximations in the Schrödinger picture reads

$$\hat{H}_I = -\hat{\sigma}^\dagger \vec{d} \cdot \hat{\vec{E}}^{(+)}(\vec{r}_A) + \text{H.c.}, \tag{1}$$

where

$$\hat{\vec{E}}^{(+)}(\vec{r}) = \int_0^\infty d\omega \hat{\vec{E}}(\vec{r},\omega) \tag{2}$$

is the positive frequency part of the electric field operator in the presence of the nanowire with $\hat{\vec{E}}(\vec{r},\omega)$ being the Fourier component of the electric field at angular frequency ω, and $\hat{\sigma}^\dagger = |e\rangle\langle g|$ is the atomic raising operator between the ground state $|g\rangle$ and the excited state $|e\rangle$ of the atom. The negative frequency counterpart of $\hat{\vec{E}}^{(+)}(\vec{r})$ is defined as

$$\hat{\vec{E}}^{(-)}(\vec{r}) = \int_0^\infty d\omega \hat{\vec{E}}^\dagger(\vec{r},\omega). \tag{3}$$

In order to incorporate the action of the nanowire one would usually decompose the electric field operator into suitable modes of an infinitely long cylindrical nanowire embedded in empty space. This approach works well if absorption losses of the medium can be neglected as is the case for a dielectric nanofiber.[15] For nanowires however, absorption losses are important and cannot be neglected. We therefore follow a different approach based on the quantization of the electromagnetic field in the presence of a lossy, passive, linear medium.[16,17] In this approach treatment the electric field operator can be expressed in terms of elementary excitations operators $\hat{\vec{f}}_\omega(\vec{r})$ and $\hat{\vec{f}}^\dagger_\omega(\vec{r})$ fulfilling bosonic commutation relations

$$[\hat{f}_{\omega_i}(\vec{r}), \hat{f}^\dagger_{\omega'_j}(\vec{r}')] = \delta_{ij}\delta(\vec{r}-\vec{r}')\delta(\omega-\omega'), \tag{4}$$

$$[\hat{f}_{\omega_i}(\vec{r},\omega), \hat{f}_{\omega'_j}(\vec{r}',\omega')] = 0 \tag{5}$$

and with free Hamiltonian

$$\hat{H}_0^F = \int d^3\vec{r} \int_0^\infty d\omega \ \hbar\omega \hat{\vec{f}}^\dagger_\omega(\vec{r}) \hat{\vec{f}}_\omega(\vec{r},\omega). \tag{6}$$

The positive frequency components ($\omega > 0$) of the electric field are given by

$$\hat{\vec{E}}(\vec{r},\omega) = i\sqrt{\frac{\hbar}{\pi\epsilon_0}}\frac{\omega^2}{c^2}\int d^3\vec{r}' \sqrt{\epsilon''(\vec{r}',\omega)}\bar{\bar{G}}(\vec{r},\vec{r}',\omega)\hat{\vec{f}}_\omega(\vec{r}'), \tag{7}$$

where $\bar{\bar{G}}(\vec{r},\vec{r}',\omega)$ is the Green's tensor of the classical field. It obeys the Maxwell-Helmholtz wave equation with a Dirac delta source at $\vec{r}=\vec{r}'$

$$\left[\nabla\times\nabla\times - \frac{\omega^2}{c^2}\epsilon(\vec{r},\omega)\right]\bar{\bar{G}}(\vec{r},\vec{r}',\omega) = \bar{\bar{I}}\delta(\vec{r}-\vec{r}'). \tag{8}$$

$\epsilon(\vec{r},\omega)$ is the relative complex dielectric function of the isotropic linear medium at position $\vec{r}$ and frequency ω, and ϵ'' denotes its imaginary part $\epsilon'' = \mathrm{Im}[\epsilon(\vec{r},\omega)]$. In the following, we will use $\epsilon = -50 + 0.6i$ as typical value inside the wire which corresponds to the electric permittivity of silver at around $\lambda = 1$ μm. Outside the wire we will assume that the field is in vacuum and it is assumed that the magnetic response is negligible.

The approach used here reduces the problem to the calculation of the classical Green's tensor of the lossy nanowire. We consider a cylindrical wire with radius R and symmetry axis z. The metal is described by a complex dielectric function with $\epsilon' = \mathrm{Re}[\epsilon] < 0$. For simplicity we assume an infinitely long wire to have translational invariance along the z axis. If the source point $\vec{r}'$ is outside the cylinder we can decompose the Green's tensor into

$$\bar{\bar{G}}(\vec{r},\vec{r}',\omega) = \begin{cases} \bar{\bar{G}}_0(\vec{r},\vec{r}',\omega) + \bar{\bar{G}}_R(\vec{r},\vec{r}',\omega) & r > R \\ \bar{\bar{G}}_T(\vec{r},\vec{r}',\omega) & r < R, \end{cases} \tag{9}$$

where r is the distance from the wire axis. If the observation point $\vec{r}$ is also outside the cylinder, we have the sum of a direct (or vacuum) contribution $\bar{\bar{G}}_0$ and a reflected contribution $\bar{\bar{G}}_R$, whereas inside the cylinder we only get a transmitted term $\bar{\bar{G}}_T$. To fulfill the boundary conditions, we expand the Green's tensor in cylindrical harmonics.[18] The cylindrical harmonic vector wave functions are given by

$$\begin{Bmatrix} \vec{M}_{e,n}(k_z,\vec{r}) \\ \vec{M}_{o,n}(k_z,\vec{r}) \end{Bmatrix} = \begin{Bmatrix} \nabla\times[Z_n(k_{r_{0,1}}r)(\cos n\phi)e^{ik_z z}\hat{z}] \\ \nabla\times[Z_n(k_{r_{0,1}}r)(\sin n\phi)e^{ik_z z}\hat{z}] \end{Bmatrix},$$

$$\begin{Bmatrix} \vec{N}_{e,n}(k_z,\vec{r}) \\ \vec{N}_{o,n}(k_z,\vec{r}) \end{Bmatrix} = \begin{Bmatrix} \frac{1}{k_{0,1}}\nabla\times\vec{M}_{e,n}(k_z,\vec{r}) \\ \frac{1}{k_{0,1}}\nabla\times\vec{M}_{o,n}(k_z,\vec{r}) \end{Bmatrix} \tag{10}$$

with $k_0 = \frac{\omega}{c}$, $k_1 = \sqrt{\epsilon_1}k_0$, and $k_{r_{0,1}}^2 = k_{0,1}^2 - k_z^2$ where we have 0,1 for outside and inside the cylinder and the subscripts e and o stand for even and odd, respectively. Note that k_1 is complex due to the nonvanishing imaginary part of the electric permittivity $\epsilon'' = \mathrm{Im}[\epsilon]$. The radial part $Z_n(x)$ has to be either replaced by the Bessel function $J_n(x)$, or, when the "(1)" appears as a superscript on $\vec{M}$ or $\vec{N}$, by $H_n^{(1)}(x)$, i.e., the Hankel function of the first kind. Note, furthermore, that the tensorial products between the even and odd cylindrical vector wave functions are defined according to $\vec{M}_{\substack{o\\e}n}\vec{N}^{(1)}_{\substack{e\\o}n} = \vec{M}_{e,n}\vec{N}^{(1)}_{o,n} + \vec{M}_{o,n}\vec{N}^{(1)}_{e,n}$ and all other combinations similarly. For better readability, we have omitted the tensorial product symbol between them.

This gives for the direct term of the Green's tensor

$$\bar{\bar{G}}_0(\vec{r},\vec{r}',\omega) = -\frac{\hat{r}\hat{r}\delta(\vec{r}-\vec{r}')}{k_0^2} + \frac{i}{8\pi}\int_{-\infty}^{\infty} dk_z \sum_{n=0}^{\infty}\frac{2-\delta_{n,0}}{k_{r_0}^2} \times \begin{cases} \vec{M}^{(1)}_{\substack{e^n\\o}}(k_z,\vec{r})\vec{M}_{\substack{e^n\\o}}(-k_z,\vec{r}') + \vec{N}^{(1)}_{\substack{e^n\\o}}(k_z,\vec{r})\vec{N}_{\substack{e^n\\o}}(-k_z,\vec{r}') \\ \vec{M}_{\substack{e^n\\o}}(k_z,\vec{r})\vec{M}^{(1)}_{\substack{e^n\\o}}(-k_z,\vec{r}') + \vec{N}_{\substack{e^n\\o}}(k_z,\vec{r})\vec{N}^{(1)}_{\substack{e^n\\o}}(-k_z,\vec{r}') \end{cases}, \tag{11}$$

where the upper (lower) line holds for $r > r'$ ($r < r'$). For the reflected part we find

$$\bar{\bar{G}}_R(\vec{r},\vec{r}',\omega) = \frac{i}{8\pi}\int_{-\infty}^{\infty} dk_z \sum_{n=0}^{\infty} \frac{2-\delta_{n,0}}{k_{r_0}^2}\{[A_R\vec{M}_{e_o^n}^{(1)}(k_z,\vec{r}) + B_R\vec{N}_{e_o^n}^{(1)} \times(k_z,\vec{r})]\vec{M}_{e_o^n}^{(1)}(-k_z,\vec{r}') + [C_R\vec{N}_{e_o^n}^{(1)}(k_z,\vec{r}) + D_R\vec{M}_{e_o^n}^{(1)} \times(k_z,\vec{r})]\vec{N}_{e_o^n}^{(1)}(-k_z,\vec{r}')\}. \quad (12)$$

Finally, we have for the transmitted part

$$\bar{\bar{G}}_T(\vec{r},\vec{r}',\omega) = \frac{i}{8\pi}\int_{-\infty}^{\infty} dk_z \sum_{n=0}^{\infty} \frac{2-\delta_{n,0}}{k_{r_0}^2}\{[A_T\vec{M}_{e_o^n}(k_z,\vec{r}) + B_T\vec{N}_{e_o^n}(k_z,\vec{r})]\vec{M}_{e_o^n}^{(1)}(-k_z,\vec{r}') + [C_T\vec{N}_{e_o^n}(k_z,\vec{r}) + D_T\vec{M}_{e_o^n}(k_z,\vec{r})]\vec{N}_{e_o^n}^{(1)}(-k_z,\vec{r}')\}. \quad (13)$$

The reflection and transmission coefficients $A_{R,T}, B_{R,T}, C_{R,T}, D_{R,T}$ can be specified by imposing the boundary conditions at the surface of the cylinder ($r=R$)

$$\hat{r}\times\bar{\bar{G}}(\vec{r},\vec{r}')_{r=R^-} = \hat{r}\times\bar{\bar{G}}(\vec{r},\vec{r}')_{r=R^+}, \quad (14)$$

$$\hat{r}\times\nabla\times\bar{\bar{G}}(\vec{r},\vec{r}')_{r=R^-} = \hat{r}\times\nabla\times\bar{\bar{G}}(\vec{r},\vec{r}')_{r=R^+}. \quad (15)$$

Solving the above equations, we get the full Green's tensor.

B. Longitudinal modes

Let us first discuss the solution of the boundary equations in the absence of material losses, i.e., for $\epsilon''=0$. Writing up Eqs. (14) and (15), one finds a system of linear algebraic equations for the transmission and reflection coefficients $A_{R,T}, B_{R,T}, C_{R,T}, D_{R,T}$. One can rewrite these as a vector, containing the coefficients, multiplied by a matrix. In order for the equations to have a nontrivial solution infinitely far from the source (i.e., where we can neglect the contribution from $\bar{\bar{G}}_0$), the determinant of the matrix has to vanish. From this condition we obtain a mode equation for each harmonic order n. These mode equations are equivalent to those obtained by different methods in Refs. 1 and 2

$$\frac{n^2k_z^2}{R^2}\left(\frac{1}{k_{r_1}^2}-\frac{1}{k_{r_0}^2}\right)^2 = \left[\frac{1}{k_{r_1}}\frac{J_n'(k_{r_1}R)}{J_n(k_{r_1}R)} - \frac{1}{k_{r_0}}\frac{H_n'(k_{r_0}R)}{H_n(k_{r_0}R)}\right] \times \left[\frac{k_1^2}{k_{r_1}}\frac{J_n'(k_{r_1}R)}{J_n(k_{r_1}R)} - \frac{k_0^2}{k_{r_0}}\frac{H_n'(k_{r_0}R)}{H_n(k_{r_0}R)}\right]. \quad (16)$$

For a given frequency ω, we get an equation for the longitudinal component of the wavevector parallel to the wire, the roots giving the allowed values $k_z=k_z(\omega;n)$ for each transversal mode n. These are the surface plasmons modes. In Fig. 1 the allowed values of k_z are plotted as function of wire radius R for the different cylindrical harmonics. One recognizes that with the shrinking of R, all solutions belonging to the $n\neq 0$ modes have a cutoff and only the one belonging to $n=0$ persists. The corresponding value of k_z diverges as $1/R$ for $R\to 0$. This divergency of k_z is associated with a strong confinement of the field around the wire: When k_z diverges, $k_{r0}=\sqrt{k_0^2-k_z^2}$ attains a large imaginary value. Since the radial confinement is mainly determined by $H_n^{(1)}(k_{r0}r)\sim\exp(ik_{r0}r)$, the divergence of k_z means that the field is confined to radial distance proportional to R. Unlike dielectric waveguides conducting waveguides thus allow for a strong confinement of the electromagnetic field around the waveguide. As we will show below, this feature enables a strong coupling between atoms and propagating plasmon modes.

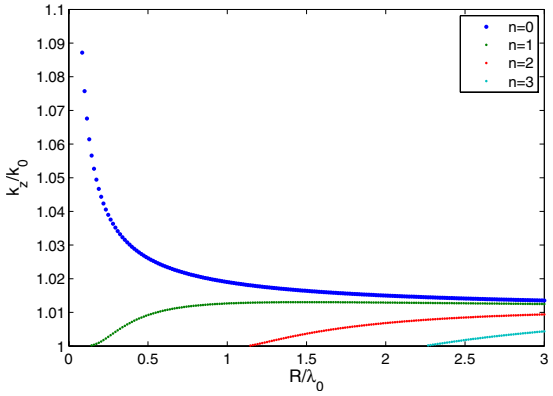

FIG. 1. (Color online) k_z components of the guided modes of a nanowire ($\epsilon=-50$), as the function of the wire radius R and cylindrical harmonic order n. When the radius decreases, all modes with a nonzero n have a cutoff, whereas the $n=0$ mode has an increasing k_z, that is, an increasingly strong confinement. R is scaled with the vacuum radiation wavelength λ_0.

When calculating the reflected and transmitted Green's tensors in Eqs. (12) and (13), the terms inside the integral and the sum $[\bar{\bar{G}}^n(\vec{r},\vec{r}',\omega;k_z)]$ have (in the absence of losses) a singularity exactly at $k_z=k_z(\omega;n)$. This singularity is a contribution to the response of the nanowire system that originates from the nth plasmonic mode.

C. Width of the plasmon resonances

Taking into account the medium absorption, i.e., a small but finite value of ϵ'', the discrete cylindrical modes turn into resonances. This means that in case of losses there is no longer a single, well-defined k_z but continuously many k_z values peaked around $k_z(\omega;n)$ that contribute to the plasmon mode. The consequences of this can be drawn much clearer if the wire radius is much smaller than the optical wavelength, because then we can interpret the propagation of the plasmon mode as a one-dimensional problem, looking at a single mode only. The material losses induce a distribution of components with different k_z values in the propagating plasmonic mode, each acquiring a phase factor $\exp(ik_zz)$ while propagating a distance z. This, in turn, results in a dephasing of the components upon propagation, which describes the losses.

Figure 2 shows the shape of the resonance belonging to the $n=0$ cylindrical mode around $k_z=\pm k_z(\omega;n)$, the value corresponding to the lossless case. The lineshape is well approximated with a Lorentzian function. The half-width at half maximum (HWHM) of the resonance peak scales lin-

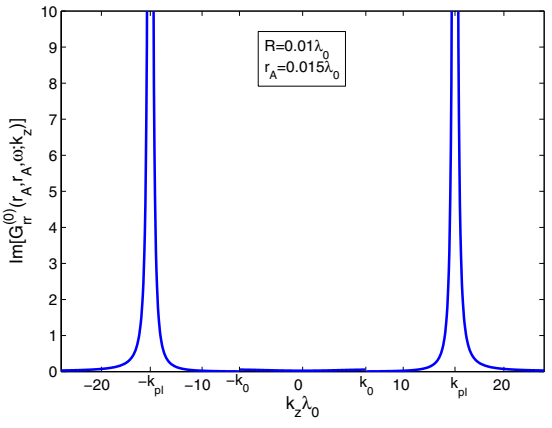

FIG. 2. (Color online) $\mathrm{Im}[\hat{r}^T \bar{\bar{G}}^{(n=0)}(\vec{r}_A, \vec{r}_A, \omega; k_z)\hat{r}]$, in case of a single-mode, lossy wire ($\epsilon = -50 + 0.6i$). $\hat{r}$ is the unit vector in the radial direction. The broadened plasmonic resonance peaks show up at around the plasmonic longitudinal wavenumbers $\pm k_{pl}$ [predicted by Eq. (16)], in the evanescent region ($k_{pl} > k_0$). The distances and wave numbers are scaled with the vacuum radiation wavelength λ_0.

early with ϵ'', as one would expect. In Fig. 3 the value of the HWHM is depicted, which assumes larger and larger values as the wire radius R gets smaller. One recognizes a transition from a slower $R^{-1/2}$ to a faster $R^{-3/2}$ dependence of the width of the plasmon resonances at around $R \sim 10^{-1}\lambda_0$.

So, in case of $\epsilon'' \neq 0$, decreasing the wire radius is accompanied not only by a decreasing transverse mode area but also by increasing propagation losses. The two effects are connected because the smaller the transverse mode area gets, the larger part of the propagating field will be concentrated inside the metal which induces increased propagation losses. We will see later that for a decreasing value of R the detrimental effects of propagation losses will overcome the positive effect of an increased coupling, resulting in an optimal wire radius.

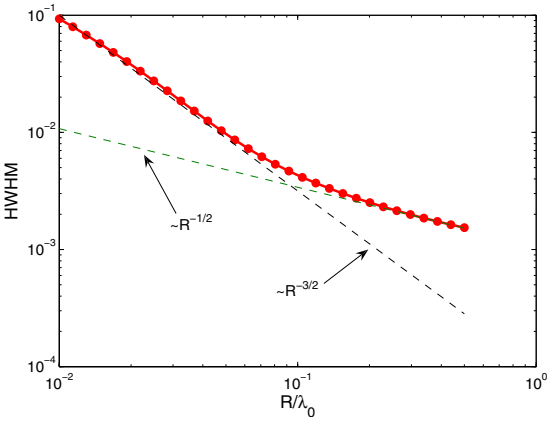

FIG. 3. (Color online) HWHM of the plasmonic resonance peaks shown in Fig. 2, as a function of wire radius R, in a log-log plot. The width and the radius are scaled by vacuum radiation wavelength λ_0. The electric permittivity is $\epsilon = -50 + 0.6i$. As the wire gets thinner, the broadening of the resonance increases, i.e., the propagation losses increase.

D. Spontaneous emission and level shift of an atom near a nanowire

It is well known that a dielectric body near an atom influences its spontaneous emission rate. The interaction strength of an atom with the different modes of the electromagnetic field is inversely proportional to the square root of the effective mode volume. That also means that the probability of spontaneous emission into modes with the smallest effective mode volume will be the largest. Additionally, slow group velocity of the given mode also enhances the interaction strength.

In the following we will take a look at the spontaneous emission rate of a two-level atom near the surface of a nanowire. We have seen before that it is possible to have a wire with a single, strongly confined mode at a given frequency, that is, a mode with a very small effective cross section area. Thus, we expect that if we place the atom close enough to the wire, its spontaneous emission rate will increase considerably.[1,2] To ascertain this, we write up the Heisenberg equations of motion for the field and atomic operators using the Hamiltonian in Eqs. (1) and (6)

$$\dot{\hat{\sigma}}_z = \frac{2i}{\hbar}\hat{\sigma}^\dagger \hat{\vec{E}}^{(+)}(\vec{r}_A, t)\cdot\vec{d} + \mathrm{H.c.}, \tag{17}$$

$$\dot{\hat{\sigma}}^\dagger = i\omega_A \hat{\sigma}^\dagger + \frac{i}{\hbar}\hat{\vec{E}}^{(-)}(\vec{r}_A, t)\cdot\vec{d}\hat{\sigma}_z, \tag{18}$$

where the operator of the electric field is given by Eq. (7). Similarly we also find the equation of motion of the elementary excitations $\hat{f}$

$$\dot{\hat{\vec{f}}}_\omega(\vec{r}) = -i\omega\hat{\vec{f}}_\omega(\vec{r}) + + \frac{\omega^2}{c^2}\sqrt{\frac{\epsilon''(\vec{r},\omega)}{\hbar\pi\epsilon_0}}\bar{\bar{G}}^*(\vec{r},\vec{r}_A,\omega)\vec{d}\hat{\sigma}. \tag{19}$$

To eliminate the field, we formally integrate Eq. (19) and substitute it into Eqs. (17) and (18). Employing a Markov approximation we get rid of the time integral and using the Green's tensor property[16,17]

$$\int d^3r' \frac{\omega^2}{c^2}\epsilon''(\vec{r}',\omega)\bar{\bar{G}}(\vec{r}_1,\vec{r}',\omega)\bar{\bar{G}}^\dagger(\vec{r}_2,\vec{r}',\omega) = \mathrm{Im}[\bar{\bar{G}}(\vec{r}_1,\vec{r}_2,\omega)] \tag{20}$$

we obtain the effective equations for $\hat{\sigma}_z$ and $\hat{\sigma}^\dagger$

$$\dot{\hat{\sigma}}_z = -\Gamma_{tot}(1+\hat{\sigma}_z) + \left[\frac{2i}{\hbar}\hat{\sigma}^\dagger \hat{\vec{E}}^{(+)}_{free}\cdot\vec{d} + \mathrm{H.c.}\right], \tag{21}$$

$$\dot{\hat{\sigma}}^\dagger = \left[i(\omega_A - \delta\omega) - \frac{1}{2}\Gamma_{tot}\right]\hat{\sigma}^\dagger + \frac{i}{\hbar}\hat{\vec{E}}^{(-)}_{free}\cdot\vec{d}\hat{\sigma}_z, \tag{22}$$

where $\hat{\vec{E}}^{(\pm)}_{free} = \hat{\vec{E}}^{(\pm)}_{free}(\vec{r}_A, t)$ is the free part of the field proportional to the free part of $\hat{f}$ and $\hat{f}^\dagger$. The total decay rate and the Lamb shift Γ_{tot} and $\delta\omega$ can then be expressed in terms of the electromagnetic Green's tensor

$$\Gamma_{tot} = \frac{2\omega_A^2 d_i d_j}{\hbar\epsilon_0 c^2}\mathrm{Im}[G_{ij}(\vec{r}_A,\vec{r}_A,\omega_A)], \tag{23}$$

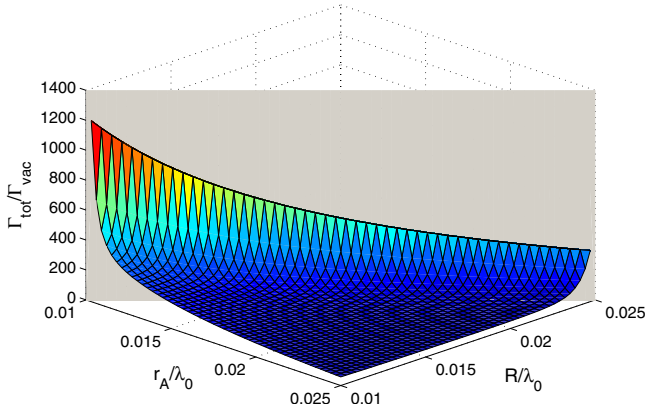

FIG. 4. (Color online) Spontaneous decay rate of a single emitter relative to the vacuum spontaneous decay rate as a function of emitter-wire axis distance r_A and wire radius R, both scaled by vacuum radiation wavelength λ_0. We use $\epsilon=-50+0.6i$. Because of the strong interaction of the emitter with the wire eigenmodes, there is a considerable increase in the spontaneous decay rate at small radii and emitter-wire distances. Since $\Gamma_{tot}\to\infty$ for $r_A\to R$, we have introduced a cutoff at a small r_A-R for better visibility.

$$\delta\omega = \frac{d_i d_j}{\hbar\epsilon_0\pi}\mathcal{P}\int_0^\infty d\omega\frac{\omega^2}{c^2}\frac{\mathrm{Im}[G_{ij}(\vec{r}_A,\vec{r}_A,\omega)]}{\omega-\omega_A}. \tag{24}$$

Figure 4 shows the results of a numerical simulation for Γ_{tot} for different atom-wire axis distances and wire radii. According to these results, the interaction of the atom with the surface plasmon mode gives rise to a significant Purcell effect, enhancing the spontaneous emission rate by 2 orders of magnitude. Thus, the atom interacts with the surface plasmon mode in the strong coupling regime. It is important to note that the interaction of the atom with the wire strongly depends on the direction of the polarization vector $\vec{d}$. The coupling to the plasmons is strongest when $\vec{d}$ points in the radial direction. In all simulations we used this configuration.

We have yet to justify the Markov approximation. In Fig. 5 we show Γ_{tot}, as a function of different atom-wire distances and frequency, taking a linear dispersion (this is a good approximation at optical frequencies). The results show that Γ_{tot} has a very large width in frequency, much more than $0.5\omega_A$, which means that the recurrence time (which is proportional to the inverse of the width) is several orders of magnitude smaller than the characteristic time scale of the atomic decay. This justifies the use of the Markov approximation.

E. Subwavelength nanowire

Although with the Green's tensor formalism one can handle the problem in an elegant way, it describes the interaction of one or many emitters with their surroundings in a compact form where contributions of different effects are difficult to distinguish. For example, when calculating the spontaneous emission of a single atom, we obtain the total emission rate into all possible modes of the environment. Thus, on first glance, the result does not enable us to separately determine the rate of spontaneous emission into electromagnetic modes associated with the nanowire plasmons and those into the radiative modes. In the following we will show, however, that with some further calculations we can still resolve the contributions of the different modes. We can separate the interaction Hamiltonian

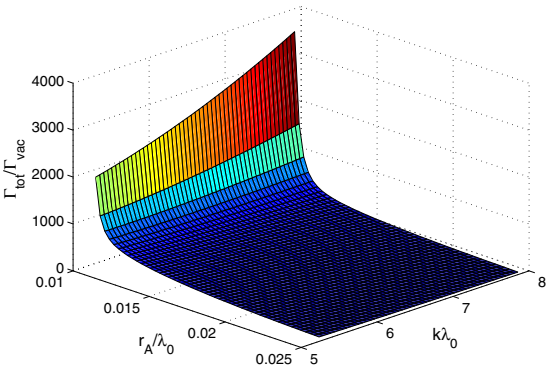

FIG. 5. (Color online) Spontaneous decay rate of a single emitter relative to the vacuum spontaneous decay rate as a function of wave number $k=\omega/c$ and emitter-wire axis distance r_A, in case of a lossy wire ($\epsilon=-50+0.6i$) with radius $R=0.01\lambda_0$. Both k and r_A are scaled by the vacuum radiation wavelength λ_0. The large width in frequency verifies the applicability of the Markov approximation. Since $\Gamma_{tot}\to\infty$ for $r_A\to R$, we have introduced a cutoff at a small r_A-R for better visibility.

$$\hat{H}_I = \hat{H}_I^{tr} + \hat{H}_I^{ev} \tag{25}$$

into a part $\hat{H}_I^{ev}$ containing the evanescent modes ($|k_z|>k_0$) and a part $\hat{H}_I^{tr}$ containing the traveling-wave part ($|k_z|\le k_0$) of the electromagnetic field. We do this because, as shown in Fig. 1, the plasmons are evanescent in the radial direction ($|k_z|>k_0$), never appearing in the traveling-wave part of the k spectrum. Moreover, for lossless media $\epsilon''=0$, one can verify from the structure of $\mathrm{Im}[\bar{\bar{G}}^{(n)}(\vec{r}_A,\vec{r}_A,\omega;k_z)]$ that the surface plasmons are the only contribution in the evanescent region. In this way we can define traveling and evanescent creation and annihilation operators $\hat{a}_\omega^{\dagger tr,ev}$, $\hat{a}_\omega^{tr,ev}$ with the usual commutation relations, so that

$$\hat{H}_I = -\int_0^\infty d\omega g^{tr}(\omega)\hat{a}_\omega^{tr}\hat{\sigma}^\dagger - \int_0^\infty d\omega g^{ev}(\omega)\hat{a}_\omega^{ev}\hat{\sigma}^\dagger + \mathrm{H.c.}, \tag{26}$$

where $g^{ev,tr}(\omega)$ is the coupling strength to the evanescent and traveling modes, respectively, at frequency ω. $\hat{\sigma}^\dagger$ is the atomic raising operator. Writing up the Heisenberg equation for $\hat{a}_\omega^{ev,tr}$ and $\hat{\sigma}$, and using that the traveling and evanescent operators commute, we get

$$\dot{\hat{a}}_\omega^{ev,tr} = -i\omega\hat{a}_\omega^{ev,tr}(t) + \frac{i}{\hbar}g^{ev,tr}(\omega)^*\hat{\sigma}(t), \tag{27}$$

$$\dot{\hat{\sigma}} = -i\omega_A\hat{\sigma}(t) - \frac{i}{\hbar}\int_0^\infty d\omega[g^{tr}(\omega)\hat{a}_\omega^{tr} + g^{ev}(\omega)\hat{a}_\omega^{ev}]\hat{\sigma}_z(t). \tag{28}$$

Formally integrating Eq. (27) and substituting into Eq. (28) yields

$$\begin{aligned}\dot{\hat{\sigma}} = &-i\omega_A\hat{\sigma}(t) - \frac{i}{\hbar}\int_0^\infty d\omega[g^{tr}(\omega)\hat{a}_\omega^{tr}(0) \\ &+ g^{ev}(\omega)\hat{a}_\omega^{ev}(0)]e^{-i\omega t}\hat{\sigma}_z(t) + \frac{1}{\hbar^2}[|g^{tr}(\omega)|^2 \\ &+ |g^{ev}(\omega)|^2]\int_{-\infty}^t d\tau\hat{\sigma}(\tau)e^{-i\omega(t-\tau)}\hat{\sigma}_z(t).\end{aligned} \tag{29}$$

Note that in Eq. (29) there are no cross terms because the traveling creation and annihilation operators commute with the evanescent ones.

We can repeat the same procedure using the Green's function formalism. For the equation of motion of $\hat{\sigma}$ we obtain

$$\begin{aligned}\dot{\hat{\sigma}} = &-i\omega_A\hat{\sigma}(t) - \frac{i}{\hbar}\int_0^\infty d\omega i\sqrt{\frac{\hbar}{\pi\epsilon_0}}\frac{\omega^2}{c^2} \\ &\times\int d^3r'\sqrt{\epsilon''(\vec{r}',\omega)}\vec{d}^T\bar{\bar{G}}(\vec{r}_A,\vec{r}',\omega)\hat{\vec{f}}_\omega(\vec{r}')\hat{\sigma}_z(t).\end{aligned} \tag{30}$$

By formal integration, we express the solution of Eq. (19) and substitute it into Eq. (30). Using the Green's function property in Eq. (20) for nonmagnetic materials we obtain the following expression:

$$\begin{aligned}\dot{\hat{\sigma}} = &-i\omega_A\hat{\sigma} - \frac{i}{\hbar}\hat{\vec{E}}_{free}^{(+)}(\vec{r}_A,t)\cdot\vec{d}\hat{\sigma}_z(t) \\ &+ \frac{1}{\hbar^2}\int_0^\infty d\omega\frac{\hbar\omega^2}{\pi\epsilon_0c^2}\vec{d}^T\,\mathrm{Im}[\bar{\bar{G}}(\vec{r}_A,\vec{r}_A,\omega)]\vec{d} \\ &\times\int_{-\infty}^t d\tau\hat{\sigma}(\tau)e^{-i\omega(t-\tau)}\hat{\sigma}_z(t),\end{aligned} \tag{31}$$

which is equivalent to Eq. (29). Both the source and the observation points are in vacuum so $|\vec{k}|=k_0=\omega/c$. Furthermore, we have seen in Sec. II that we find the Green's tensor by integrating an analytic, k_z- and n-dependent expression over k_z and summing it up over n. With this we can rewrite Eq. (31) such that it assumes the form

$$\begin{aligned}\dot{\hat{\sigma}} = &-i\omega_A\hat{\sigma} - \frac{i}{\hbar}\hat{\vec{E}}_{free}^{(+)}(\vec{r}_A,t)\cdot\vec{d}\hat{\sigma}_z(t) \\ &+ \frac{1}{\hbar^2}\int_0^\infty d\omega\int_{-\infty}^\infty dk_z\sum_{n=0}^\infty\frac{\hbar\omega^2}{\pi\epsilon_0c^2}\vec{d}^T\,\mathrm{Im}[\bar{\bar{G}}^{(n)}(\vec{r}_A,\vec{r}_A,\omega;k_z)]\vec{d} \\ &\times\int_{-\infty}^t d\tau\hat{\sigma}(\tau)e^{-i\omega(t-\tau)}\hat{\sigma}_z(t).\end{aligned} \tag{32}$$

Comparing Eqs. (29) and (32), separating the evanescent and traveling contributions, and exploiting the symmetry of $\mathrm{Im}[\bar{\bar{G}}^{(n)}(\vec{r}_A,\vec{r}_A,\omega;k_z)]$ in k_z we can identify

$$|g^{ev}(\omega)|^2 = 2\int_{k_0}^\infty dk_z\sum_{n=0}^\infty\frac{\hbar\omega^2}{\pi\epsilon_0c^2}\times\vec{d}^T\,\mathrm{Im}[\bar{\bar{G}}^{(n)}(\vec{r}_A,\vec{r}_A,\omega;k_z)]\vec{d}, \tag{33}$$

$$|g^{tr}(\omega)|^2 = 2\int_0^{k_0} dk_z\sum_{n=0}^\infty\frac{\hbar\omega^2}{\pi\epsilon_0c^2}\times\vec{d}^T\,\mathrm{Im}[\bar{\bar{G}}^{(n)}(\vec{r}_A,\vec{r}_A,\omega;k_z)]\vec{d}. \tag{34}$$

According to Fermi's golden rule, the square of the coupling strength to a given mode of the field is proportional to the spontaneous decay rate into that mode. Because of this and Eqs. (33) and (34), we can define the decay rate into the plasmon mode associated with the nth cylindrical order

$$\begin{aligned}\Gamma_{pl}(\omega) &= \sum_{n=0}^\infty 2\int_{k_0}^\infty dk_z\frac{2\omega^2}{\hbar\epsilon_0c^2}\vec{d}^T\,\mathrm{Im}[\bar{\bar{G}}^{(n)}(\vec{r}_A,\vec{r}_A,\omega;k_z)]\vec{d} \\ &= \sum_{n=0}^\infty\Gamma_{pl}^{(n)}(\omega).\end{aligned} \tag{35}$$

The above decomposition into traveling and plasmonic components is strictly valid only in the absence of losses. In case of a lossy wire, the plasmon resonances will not be singularities anymore but finite peaks with a finite width. Moreover, they will no longer be the only contribution in the evanescent region: apart from the resonance peaks, we observe a broad, low-amplitude background that is due to dissipative local circulating currents. As shown in Ref. 19, $\epsilon''\neq 0$ results in nonradiative losses which, in turn, have a contribution to $|g^{tr}(\omega)|^2$, and, because of the circulating currents, also to $|g^{ev}(\omega)|^2$. Our main interest lies in a thin, single-mode wire where we do not have higher order plasmon modes (see Fig. 1). This allows us to resolve the plasmon mode from the circulating surface currents to a good approximation. The evanescent part of the $n>0$ cylindrical orders contains only the circulating current background. As for the $n=0$ contribution, one can verify that there is no peak-sitting-on-a-background behavior in $\mathrm{Im}[\bar{\bar{G}}^{(n=0)}(\vec{r}_A,\vec{r}_A,\omega;k_z)]$, but instead we have a single peak, corresponding to the plasmon mode, with an almost perfect Lorentzian shape. So, in the $n=0$ contribution we have no, or negligible circulating surface current contribution. Thus, in the single-mode case the decay rate into the plasmon mode can be calculated as

$$\Gamma_{pl}(\omega) = 2\int_{k_0}^\infty dk_z\frac{2\omega^2}{\hbar\epsilon_0c^2}\vec{d}^T\,\mathrm{Im}[\bar{\bar{G}}^{(n=0)}(\vec{r}_A,\vec{r}_A,\omega;k_z)]\vec{d}. \tag{36}$$

We plot the emission rate into the plasmons normalized to the overall decay rate as a function of the atomic distance from the wire axis in Fig. 6. For small atom-wire distances, the decay rate goes almost entirely into the plasmonic mode which reveals the extraordinarily strong coupling achievable in near-field plasmonic systems.[1,2] Furthermore, we observe

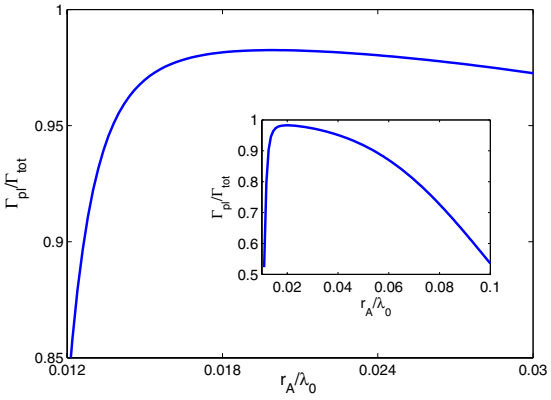

FIG. 6. (Color online) Spontaneous emission rate into the plasmon mode relative to the total spontaneous decay rate, as a function of source distance from the wire axis r_A, scaled by the vacuum radiation wavelength λ_0, in case of a wire of radius $R=0.01\lambda_0$ and $\epsilon=-50+0.6i$. There is an optimal r_A at which the coupling of a single emitter to the plasmon mode is maximal. The inset shows the behavior of the relative decay rate over a larger interval of r_A values.

that there is an optimum distance at which this value is maximal. This is in accordance with the result in Refs. 1 and 2. Our description enables us to determine the origin of this effect. If the atom gets far from the wire, the spontaneous emission rate into the confined plasmon modes decreases rapidly, while the emission rate into the traveling modes stays more or less constant (practically zero reflection from the wire and constant vacuum spontaneous emission rate) which results in an overall decrease in Γ_{pl}/Γ_{tot}. Close to the wire the strong confinement of the plasmon modes enhances the coupling to the plasmon mode such that the decay is almost exclusively into the guided mode. If the atom gets too close to the wire, however, the near field circulating current contribution increases faster than the decay rate into the $n=0$ plasmon mode. This, again, leads to an overall decrease in the relative decay rate.

III. WIRE-MEDIATED INTERACTION OF EMITTERS

A. Subradiant and superradiant coupling mediated by the nanowire

If we place two emitters along the single-mode wire, both at the same distance from the surface, close enough to couple to the single surface plasmon mode, they will have a long-range interaction mediated by the plasmons. In the following, we will investigate this interaction. The rotating-wave Hamiltonian of two identical, two-level atoms interacting with the environment, i.e., with the elecromagnetic field in presence of the nanowire, in the dipole approximation assumes the form

$$\hat{H} = \int d^3\vec{r} \int_0^\infty d\omega \hbar\omega \hat{\vec{f}}_\omega^\dagger(\vec{r}) \hat{\vec{f}}_\omega(\vec{r}) + \frac{1}{2}\hbar\omega_A(\hat{\sigma}_{z1} + \hat{\sigma}_{z2}) + [-\hat{\sigma}_1^\dagger \hat{\vec{E}}^{(+)}(\vec{r}_1,t)\vec{d}_1 - \hat{\sigma}_2^\dagger \hat{\vec{E}}^{(+)}(\vec{r}_2,t)\vec{d}_2 + \text{H.c.}], \quad (37)$$

where the indices 1 and 2 refer to the first and second atom. Here the first term represents the field energy in the presence of the nanowire. The field is represented by the elementary excitations operators $\hat{\vec{f}}_\omega$ and $\hat{\vec{f}}_\omega^\dagger$, which are related to the electric field through Eq. (7). Since Eq. (7) involves the full Green's function the interaction of the field with the nanowire is already incorporated in the definition of $\hat{\vec{f}}_\omega$ and $\hat{\vec{f}}_\omega^\dagger$. This is the main advantage of the Green's function formalism. Note that although describing the combined field-plus-nanowire system, the operators $\hat{\vec{f}}_\omega$ and $\hat{\vec{f}}_\omega^\dagger$ satisfy the free-field commutation relations in Eq. (5).[16,17] The second term in the Hamiltonian represents the atomic energy and the second line describes the interaction between the atoms and the field excitations through Eq. (7). In Sec. II D we proceeded by deriving the Heisenberg equations of motion for a single atom coupled to the wire. For the present purpose it is more desirable to work in the Schrödinger picture but the method used is equivalent to the description in Sec. II D: similarly to the treatment in Refs. 20 and 21, we write up the master equation, trace out the reservoir and after applying Born and Markov approximations we get the equation of motion for the reduced, two-atom density matrix

$$\dot{\hat{\rho}} = -\sum_{k,l=1}^{2} \frac{\Gamma_{kl}}{2}(\hat{\sigma}_l^\dagger \hat{\sigma}_k \hat{\rho} + \hat{\rho}\hat{\sigma}_l^\dagger \hat{\sigma}_k - 2\hat{\sigma}_k \hat{\rho} \hat{\sigma}_l^\dagger) + i\sum_{k,l=1}^{2} \delta\omega_{k,l}[\hat{\sigma}_l^\dagger \hat{\sigma}_k, \rho]. \quad (38)$$

Here $\delta\omega_{kk}$ are the single-atom Lamb shifts and $\delta\omega_{12}$ is the radiative dipole-dipole shift. Similarly, Γ_{kk} is the single-atom decay rate Γ_{tot} derived in Sec. II D and Γ_{12} is a contribution which describes the effect of atoms upon each other

$$\Gamma_{12} = \frac{2\omega_A^2 d_{1i} d_{2j}}{\hbar\epsilon_0 c^2} \text{Im}[G_{ij}(\vec{r}_1, \vec{r}_2, \omega_A)], \quad (39)$$

$$\delta\omega_{12} = \frac{d_{1i} d_{2j}}{\hbar\epsilon_0 \pi} \mathcal{P} \int_0^\infty d\omega \frac{\omega^2}{c^2} \frac{\text{Im}[G_{ij}(\vec{r}_1, \vec{r}_2, \omega)]}{\omega - \omega_A}. \quad (40)$$

The one-atom flip operators have the form $\hat{\sigma}_k = |g\rangle_{kk}\langle e|$ with $|g\rangle_k$ being the ground state and $|e\rangle_k$ the excited state of the kth atom. The calculation of the dipole-dipole shift involves the integration of the Green's tensor in frequency space and is a bit involved. It will thus be disregarded in the following discussion. The shift mediated by the nanowire is typically at most on the order of the linewidth of the transition if the distance is larger than the plasmon wavelength. Taking it into account would slightly improve the fidelity of the phase gate discussed below.

Since $\Gamma_{21}=\Gamma_{12}$, Eq. (38) is diagonal in the basis of symmetrized and antisymmetrized states, namely, $|ee\rangle$, $|S\rangle = (|ge\rangle + |eg\rangle)/\sqrt{2}$, $|AS\rangle = (|ge\rangle - |eg\rangle)/\sqrt{2}$, and $|gg\rangle$. Writing up the equations of motion for the populations of these states we get

$$\dot{\rho}_{ee}^{ee} = -2\Gamma_{11}\rho_{ee}^{ee}, \quad (41)$$

$$\dot{\rho}_S^S = (\Gamma_{11} + \Gamma_{12})\rho_{ee}^{ee} - (\Gamma_{11} + \Gamma_{12})\rho_S^S, \quad (42)$$

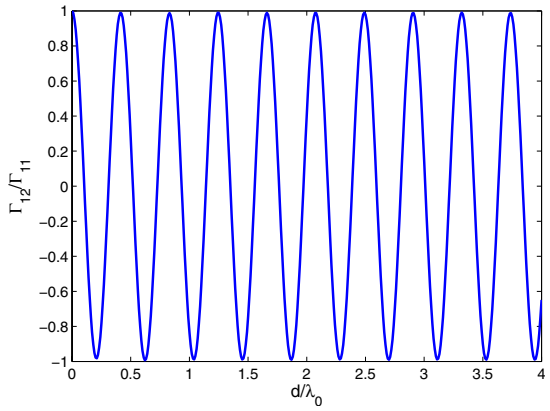

FIG. 7. (Color online) Variation in Γ_{12}/Γ_{11} as a function of the distance d between two emitters, in a lossless, single-mode wire of radius $R=0.01\lambda_0$. The emitter-wire axis distance is $r_A=0.015\lambda_0$. The oscillations result in the alternation between superradiance and subradiance of the symmetric and antisymmetric atomic transitions. All distances are scaled by the vacuum radiation wavelength λ_0.

$$\dot{\rho}_{AS}^{AS} = (\Gamma_{11} - \Gamma_{12})\rho_{ee}^{ee} - (\Gamma_{11} - \Gamma_{12})\rho_{AS}^{AS}, \tag{43}$$

$$\dot{\rho}_{gg}^{gg} = (\Gamma_{11} + \Gamma_{12})\rho_{S}^{S} + (\Gamma_{11} - \Gamma_{12})\rho_{AS}^{AS}. \tag{44}$$

We have here used the notation that the matrix elements of the two-particle density operator are $\rho_{es}^{gs}=\langle gs|\hat{\rho}|es\rangle$. Additionally, from the equations of the coherences, we perceive that the resonance frequency of $|AS\rangle$ has been shifted downwards by $\delta\omega_{12}$, whereas that of $|S\rangle$ has increased by the same amount. As we discuss below, the magnitude of Γ_{12} will be responsible for the superradiance and subradiance of the symmetric and antisymmetric transitions.

Figures 7 and 8 show the value of the cross relaxation rate Γ_{12} normalized to the single-atom decay rate $\Gamma_{11}=\Gamma_{22}$, where we have varied the distance between the two atoms by several vacuum wavelengths while keeping the atom-wire distance constant with metal losses switched off and on, respectively. We observe an oscillatory behavior of Γ_{12} between $\pm\Gamma_{11}$, where the period of oscillations matches exactly the longitudinal wavelength of the surface plasmon mode. In essence, this effect is caused by the interference of the radiation emitted by the two atoms. If the distance between the atoms is an integer number of plasmons wavelength the emission from the two atoms will interfere constructively in the symmetric state $|S\rangle$. The decay rate $\Gamma_{11}+\Gamma_{12}$ for $|S\rangle$ will thus increase relative to the single atom decay rate ($\Gamma_{12}>0$). Similarly there will be destructive interference of the emission from the antisymmetric state $|AS\rangle$ giving rise to a decreased emission rate $\Gamma_{11}-\Gamma_{12}$. If on the other hand the distance between the atoms is a half integer number of wavelengths the constructive interference is from the antisymmetric state $|AS\rangle$ corresponding to $\Gamma_{12}<0$. Note that the physical decay rates (eigenvalues of the decay matrix) given by $\Gamma_{11}\pm\Gamma_{12}$ are always non-negative despite the sign of Γ_{12}. Besides, one can see in Fig. 7 that the maximum value of Γ_{12} is very close to Γ_{11} which means an efficient enhancement/suppression of spontaneous decay of the corresponding transitions. Therefore, the atoms are indeed strongly coupled to the guided mode—not only is the overall decay rate greatly enhanced but almost the whole of the radiated energy is carried by the plasmons. If there are losses in the metal, however, the oscillations are damped as shown in Fig. 8.

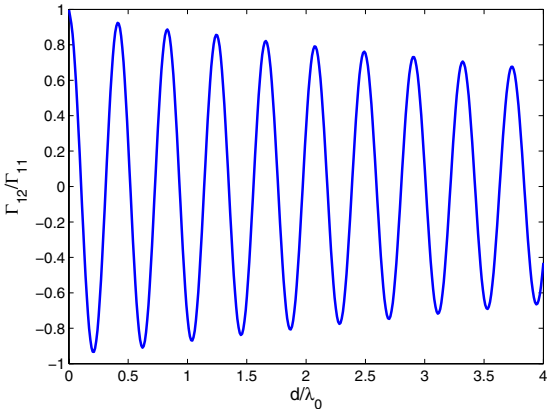

FIG. 8. (Color online) Variation in Γ_{12}/Γ_{11} as a function of the distance d between two emitters, in a single-mode, lossy wire ($\epsilon=-50+0.6i$) of radius $R=0.01\lambda_0$. The emitter-wire axis distance is $r_A=0.015\lambda_0$. The oscillation is damped because of the dissipation of plasmons upon propagation. All distances are scaled by the vacuum radiation wavelength λ_0.

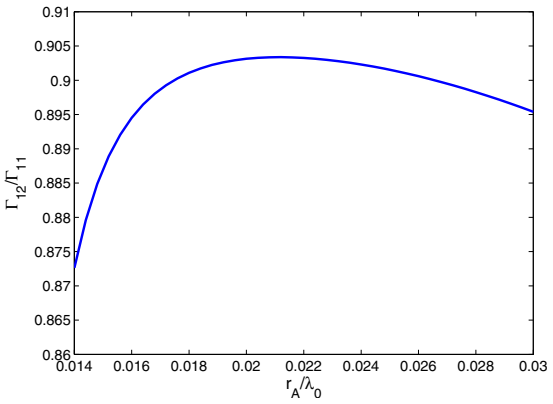

FIG. 9. (Color online) Magnitude of an extremal value of Γ_{12}/Γ_{11} as the function of the atom-wire axis distance r_A, scaled by the vacuum radiation wavelength λ_0, at wire radius $R=0.01\lambda_0$ and inter-atomic distance $d=0.83\lambda_0$. We use $\epsilon=-50+0.6i$. There is an optimal r_A where the coupling to the guided mode is maximal, resulting in a minimal damping of the oscillations of Γ_{12}/Γ_{11}.

Finite material losses, i.e., $\epsilon'' \neq 0$ give rise to another effect related to the discussion in Sec. II E. If we put an emitter too close to the wire surface, nonradiative losses become increasingly important. Thus, although the coupling strength to the plasmons increases, the nonradiative channel will take over. Therefore, as Fig. 9 shows, there is, again, an optimal distance of the emitters, where the contrast of the superradiance and subradiance is maximal. However, the optimum distance is slightly different from the one found in Sec. II E. Since we have two, strongly interacting emitters, the decay rate of the two-atom system into the plasmon mode will change differently as compared to the single-atom decay rate. Because of this, one can observe that the maximum in Fig. 9 is slightly shifted compared to that of Fig. 6.

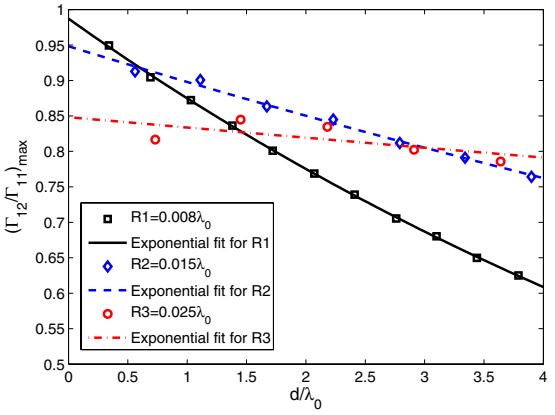

FIG. 10. (Color online) Maximal values of Γ_{12}/Γ_{11}, as a function of propagation distance d, for three different single-mode wire radii. We use $\epsilon''=-50+0.6i$. The lines are exponential fits to the Γ_{12}/Γ_{11} peak values, represented by the markers. As R decreases, the propagation losses increase but the largest achievable $(\Gamma_{12}/\Gamma_{11})_{max}$ value also gets higher. Thus, at a given interemitter distance there exists a single R that ensures a maximal strength of the interaction between the emitters along the wire.

The efficiency of the coupling between two emitters separated by a fixed distance d will depend on several factors. In order to maximize the single-atom plasmon coupling the atom should be placed as close as possible to the wire surface. Since at some point nonradiative losses of the single atom increase more rapidly when approaching the surface, there is an optimum atom-wire distance for a given wire radius R. On the other hand the propagating plasmons also experience absorption originating from the same material losses. These absorption losses depend on the structure of the mode function and thus also on the wire radius R. We have examined whether for a fixed distance d along the wire there is a wire radius allowing an optimal compromise between these two effects. In Fig. 10 we plot the enveloping curve of the maxima of Γ_{12}/Γ_{11} as a function of interatomic distance, in case of three different wire radii. In each case we used a wire-emitter distance that allowed an optimal atom-plasmon coupling. One can see that at a smaller radius R, the achievable maximum of Γ_{12}/Γ_{11} is higher. However, as the propagation distance increases, the value of the envelope decreases faster compared to the case of a larger R. According to this, if the emitters are close to each other, it is better to have a wire with a smaller radius. On the other hand, if they are further apart the optimal radius would be a larger one. There is thus an optimal wire radius for a given interatomic distance but there is no single optimal R for all cases.

The superradiance effect is sensitive to the positioning of the atoms so the experimental realization with a given atoms distance may be technically demanding. A possible method could be to use atoms trapped in very deep trapping potentials possible created by an evanescent standing wave field surrounding the nanowire.[22] Alternatively one could use impurities in a solid state material acting as artificial atoms. Ideally such impurities could be implanted at a well-determined position[23] but alternatively the effects discussed here could also be observed by post-selecting wires where, e.g., the random position of impurities match the desired distance.

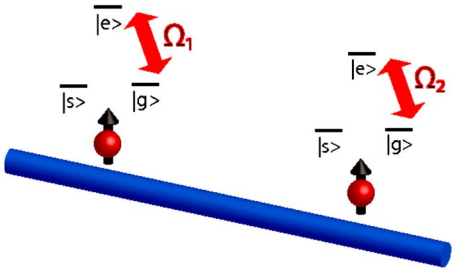

FIG. 11. (Color online) Realization of a deterministic quantum phase gate, by coupling the $|e\rangle-|g\rangle$ transitions of two λ atoms to a single surface plasmon mode, inducing superradiance in the two-atom system, and applying external classical 2π pulses.

B. Application for a phase gate

As a possible application, we are in the following going to analyze the realization of a deterministic quantum phase gate between two λ atoms coupled by a single surface plasmon mode of the nanowire, as shown in Fig. 11. We assume that only the $|g\rangle\rightarrow|e\rangle$ transition of each emitter is coupled to the single guided mode of the wire. If the two emitters are several wavelengths apart they can individually be addressed by lasers coupling the $|g\rangle\rightarrow|e\rangle$ transition. The phase gate works by exploiting the large difference in the decay rates between the superradiant and subradiant states shown in Fig. 8. Assume first that we can ignore the decay of the excited level $|e\rangle$ in the $|g\rangle-|e\rangle$ two level system. In this case it is well known that a 2π pulse, forcing the system to do a full Rabi oscillation, gives an additional π phase to the atomic system. On the other hand if the decay rate of the excited state Γ_{eg} is much stronger than the resonant Rabi frequency $\Omega\ll\Gamma$, the driving field cannot induce Rabi oscillations between the two levels, and the drive merely introduces a scattering rate $\propto\Omega^2/\Gamma_{eg}$, which vanishes in the limit of weak driving or strong decay. The idea behind the phase gate is that due to the subradiant effect we saw above, the interaction of a nearby emitter can change the excited state from being decaying into being nondecaying, thereby allowing the first emitter to pick up a π phase shift conditioned on the state of the other.

Specifically, consider the level scheme of the two-atom system shown in Fig. 12. The ground and excited state of atoms 1 and 2 are coupled by resonant classical drive fields with a strength parametrized by the Rabi frequencies Ω_1 and Ω_2, i.e., $H_i=\Omega_i(|g\rangle_i\langle e|+|e\rangle_i\langle g|)$ with $i=1$ and 2. These fields couple the states $|gg\rangle$, $|eg\rangle$, $|ge\rangle$ and $|ee\rangle$ of the combined system but it is desirable to express the interaction in the a basis involving the states $|S\rangle=(|eg\rangle+|ge\rangle)/\sqrt{2}$ and $|AS\rangle=(|eg\rangle-|ge\rangle)/\sqrt{2}$, because these states have a simpler decay dynamics, cf., Eqs. (42) and (43). In this case one gets the couplings shown in Fig. 12 with the effective coupling strengths

$$\Omega_S=\frac{1}{\sqrt{2}}(\Omega_1+\Omega_2), \tag{45}$$

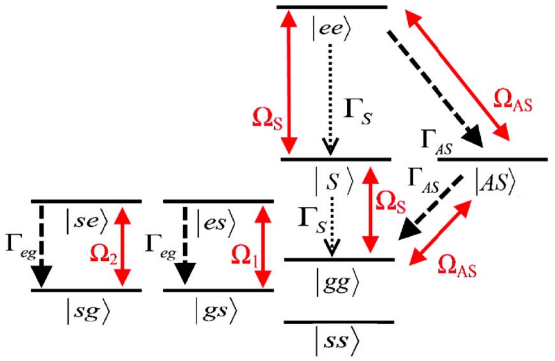

FIG. 12. (Color online) Effective level scheme of two, externally driven, interacting three-level λ atoms, seen in Fig. 11. Ω_S and Ω_{AS} are, respectively, the symmetric and antisymmetric superpositions of Ω_1 and Ω_2. Because of the strong coupling to a single plasmonic mode, a high-contrast superradiance effect is present in the system, inducing a slow decay in the symmetric transition and a fast one in the antisymmetric transition.

$$\Omega_{AS} = \frac{1}{\sqrt{2}}(\Omega_1 - \Omega_2). \tag{46}$$

Assume now that the distance between the atoms is such that the symmetric state $|S\rangle$ is subradiant whereas the antisymmetric state $|AS\rangle$ is superradiant $\Gamma_{AS} \gg \Gamma_S$ and that $\Omega_2 = \Omega_1$ corresponding to $\Omega_{AS}=0$ and $\Omega_S=\sqrt{2}\Omega_1$. Choosing the driving strength Ω_S to be in between the two decay rates

$$\Gamma_{AS} \gg \Omega_S \gg \Gamma_S \tag{47}$$

ensures that transition to the double excited state $|ee\rangle$ is blocked by the strong decay Γ_{AS}, whereas we can perform a 2π Rabi oscillation on the two-level system given by $|gg\rangle$ and $|S\rangle$ (see Fig. 12). This thus ensures that we achieve a phase change in π on the $|gg\rangle$ state. Starting from the states $|gs\rangle$ and $|sg\rangle$ there is essentially only a single atom interaction with the wire since there is no coupling to the state $|s\rangle$. The excited state therefore always has a fast decay $\Gamma_{11} \sim \Gamma_{AS}/2$ such that the driving is too weak to excite the atoms. Furthermore the state $|ss\rangle$ is completely unaffected by the classical light pulses and in the ideal limit the entire process will therefore have the truth table

$$\begin{aligned} |ss\rangle &\to |ss\rangle, \\ |sg\rangle &\to |sg\rangle, \\ |gs\rangle &\to |gs\rangle, \\ |gg\rangle &\to -|gg\rangle. \end{aligned} \tag{48}$$

In reality the finite ratio Γ_{AS}/Γ_S will limit how well one can fulfill the condition in Eq. (47) and this will limit the fidelity F of the gate. Choosing the Rabi frequency too small will lead a decay from the excited state during the 2π pulse on the $|gg\rangle - |S\rangle$ transition. This will result in an error with a probability $\propto \Gamma_S T_{\text{pulse}} \propto \Gamma_S/\Omega_1$, where the pulse duration T_{pulse} is set by $T_{\text{pulse}} \sim 1/\Omega_1$. Choosing the driving too strong will allow scattering from the transitions which are supposed to be blocked by the fast decay of the excited states with decay rates $\Gamma_S \propto \Gamma_{eg}$. This introduces an error probability $\propto T_{\text{pulse}}\Omega_1^2/\Gamma_{eg} \propto \Omega_1/\Gamma_{eg}$ resulting in a total imperfection

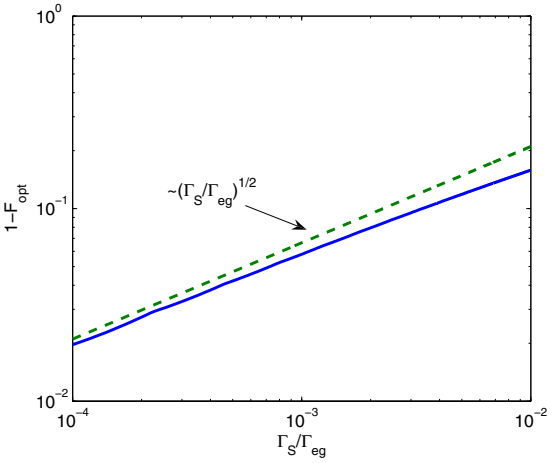

FIG. 13. (Color online) Fidelity of a maximally entangled state created by the phase gate optimized with respect to the drive strength. The phase gate fidelity error scales roughly as $\sqrt{\Gamma_S/\Gamma_{eg}}$ (dashed line) in the limit $F \to 1$.

$$1 - F \sim \frac{\Omega_1}{\Gamma_{eg}} + \frac{\Gamma_S}{\Omega_1}. \tag{49}$$

Minimizing Eq. (49) with respect to Ω_1, we find that the minimal imperfection scales as

$$1 - F_{opt} \sim \sqrt{\frac{\Gamma_S}{\Gamma_{eg}}}. \tag{50}$$

To confirm this rough scaling analysis we show in Fig. 13 the result of a full numerical simulation of the density matrix equation for the system. We can write the fidelity of the gate operation as the square of the absolute value of the overlap between the desired final atomic state and the one we get in the end

$$F = |\langle \psi_{\text{ideal}}|\psi\rangle|^2 = \langle \psi_{\text{ideal}}|\psi\rangle\langle\psi|\psi_{\text{ideal}}\rangle, \tag{51}$$

which is the expectation value of the final density operator taken in the desired atomic state

$$F = \langle \psi_{\text{ideal}}|\hat{\rho}|\psi_{\text{ideal}}\rangle. \tag{52}$$

Using $|\psi_{\text{initial}}\rangle = 1/2(|ss\rangle + |sg\rangle + |gs\rangle + |gg\rangle)$ as a starting state, in Fig. 13 we show the error $1-F$, where F is optimized over the driving strength Ω_1 as a function of the ratio of the decay rates Γ_S/Γ_{eg}. Here $|\psi_{\text{ideal}}\rangle = 1/2(|ss\rangle + |sg\rangle + |gs\rangle - |gg\rangle)$ is a maximally entangled state created using the phase gate combined with ideal $\pi/2$ pulses on the $|g\rangle - |s\rangle$ transitions. The dashed line shows the scaling derived above $1-F = c\sqrt{\Gamma_S/\Gamma_{eg}}$ with the constant c chosen to match the behavior as $F \to 1$.

The analysis of the phase gate has so far not been tied to any particular system but applies to any system where there is a large difference in the decay rates of the superradiant and subradiant states. We now turn to the specific implementation in terms of atoms coupled through the plasmon. As we saw

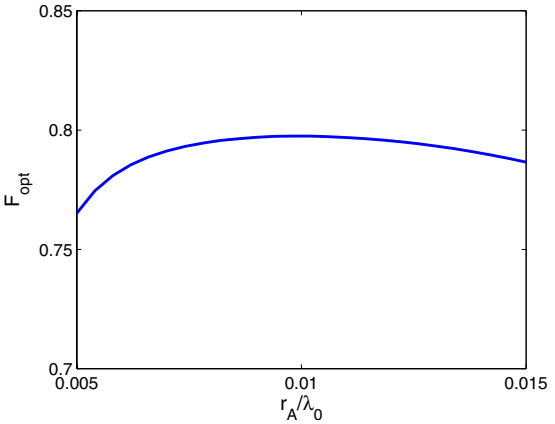

FIG. 14. (Color online) Optimal fidelity of a maximally entangled state generated with the phase gate as a function of the atom-wire axis distance r_A. r_A is scaled with the vacuum radiation wavelength λ_0. The two-atom states $|ss\rangle$, $|sg\rangle$, $|gs\rangle$, and $|gg\rangle$ are initially equally populated. We have here used the parameters $R=0.003\lambda_0$, $d=0.07\lambda_0$, and $\epsilon=-50+0.6i$ in the simulation.

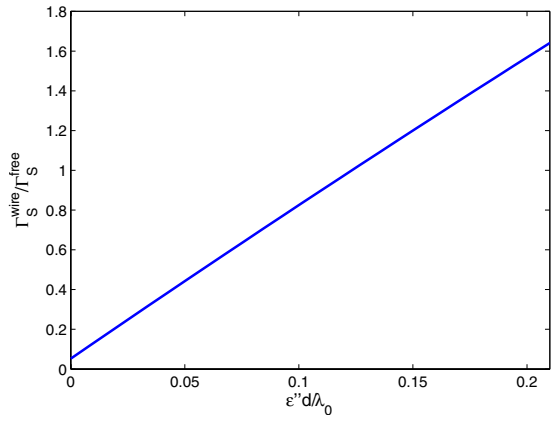

FIG. 15. (Color online) Ratio of wire-loss-induced and free-space-loss-induced contributions of Γ_S, as a function of $\epsilon'' d/\lambda_0$, where we restrict d to take up values of the distances belonging to the minima of Γ_{12}/Γ_{11} (see Fig. 8). In the region of $\Gamma_S^{wire}/\Gamma_S^{free}<1$ the gate fidelity could be considerably increased by suppressing the spontaneous radiation into free space.

above, the subradiant state does not have a completely vanishing decay rate and accordingly this will limit the fidelity of the gate. In Fig. 14, we show the optimal fidelity of the gate operation, optimized by varying Ω_S, as a function of the atom-wire axis distance r_A. For the simulation, we used $R=0.003\lambda_0$ and $d=0.07\lambda_0$.

The results show a maximum fidelity of 80% for the parameters above. There are two major detrimental effects which reduce the superradiance-subradiance contrast and, consequently, the gate fidelity, namely, the coupling to free space and the wire losses. Due to the free space coupling, a small amount of the radiated energy will be scattered into the far-field region, resulting in a nonzero contribution to Γ_S. The wire losses induce traveling wave and circulating current dissipation leading to an additional, local loss of energy. This also contributes to Γ_S. It is possible to suppress the spontaneous emission into free space, for example, by placing the atoms into a photonic bandgap material. This would considerably enhance the gate fidelity only if the free-space contribution to Γ_S is dominant with respect to the wire-loss contribution. Figure 15 shows the ratio $\Gamma_S^{wire}/\Gamma_S^{free}$ as a function of $d\epsilon''/\lambda_0$, for distances d corresponding to the minima of Γ_{12}/Γ_{11}. As one can see, to increase the interemitter distance d while keeping $\Gamma_S^{wire}/\Gamma_S^{free}<1$, we need to decrease ϵ''. For the given parameters, this means that, for instance, for $d\approx\lambda_0$ we have to have $\epsilon''\approx 0.1$. Another means of increasing the fidelity could be to build a cavity for the plasmon, e.g., by using a ring shaped wire, but this will depend on the losses of such a cavity mode, e.g., due to radiation and dissipation. A full investigation of this is beyond the scope of this paper.

C. Realization of spin-boson model

The plasmon-mediated interaction between spins along a nanowire could also be used to implement interesting and important many-body models involving a one-dimensional continuum of bosonic modes. The role of the latter is played here by the guided plasmon modes. Of particular interest is e.g., the spin-boson model,[24] in which a chain of spins is coupled to the one-dimensional continuum of bosonic modes through an interaction of the type

$$\hat{H}_{\mathrm{SB}}=\int_0^\infty d\omega\sum_j(\hat{\sigma}_j+\hat{\sigma}_j^\dagger)(g(\omega)\hat{a}_\omega+g^*(\omega)\hat{a}_\omega^\dagger). \quad (53)$$

Different from the atom-plasmon coupling in Eq. (1) discussed throughout this paper, this Hamiltonian contains counter rotating terms of the form $\hat{\sigma}^\dagger\hat{a}^\dagger$ and $\hat{\sigma}\hat{a}$. Typically these terms can be neglected for electromagnetic modes oscillating at optical frequencies, which constitutes the so-called rotating-wave approximation (RWA). It is, however, possible to compensate the fast oscillations by using effective two-photon Raman transitions rather than single-photon ones, as suggested in Ref. 25. Consider e.g., the $F=1/2-F=1/2$ coupling scheme shown in Fig. 16, where the lower state $|g\rangle$ is coupled to another state $|s\rangle$ in the ground-state manifold via a two-photon Raman transition through an excited state $|e_+\rangle$ involving a right circular polarized external drive field of Rabi frequency Ω_+ and the linear polarized quantized plasmon field $\vec{E}$. In addition the state $|s\rangle$ is coupled

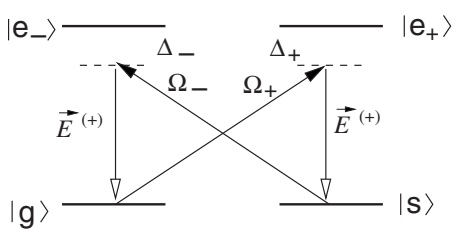

FIG. 16. Raman coupling scheme for the realization of a spin-boson model. In the rotating wave approximation the atom can make a transition from $|g\rangle$ to $|s\rangle$ either by emitting a photon into $\hat{E}$ via the transition $|g\rangle\rightarrow|e_+\rangle\rightarrow|s\rangle$ or by absorbing a photon from $\hat{E}$ via the transition $|g\rangle\rightarrow|e_-\rangle\rightarrow|s\rangle$.

through another excited state $|e_-\rangle$ via a two-photon Raman transition involving a left circular polarized external drive field Ω_- and again the linear polarized plasmon field $\vec{E}$. For each single-photon transition the rotating-wave approximation is well justified since we are considering optical fields. The complete interaction Hamiltonian in RWA thus reads

$$\hat{H}_I = \sum_j \{\hbar\Omega_+^* \hat{\sigma}^j_{e+,g} + \Omega_-^* \hat{\sigma}^j_{e-,s} + \text{H.c.}\} + \sum_j [\hat{\sigma}_{e-,g}\vec{d}_- \cdot \hat{\vec{E}}^{(+)}(z_j) + \hat{\sigma}_{e+,s}\vec{d}_+ \cdot \hat{\vec{E}}^{(+)}(z_j)]. \quad (54)$$

Here $\hat{\sigma}^j_{\mu,\nu} = |\mu\rangle_{jj}\langle\nu|$ are the atomic flip operators between states $|\nu\rangle$ and $|\mu\rangle$ of the jth atom at position z_j, and $\vec{d}_\pm$ are the vector dipole moments of the transitions $|s\rangle - -|e_+\rangle$ and $|g\rangle - -|e_-\rangle$, respectively.

It is assumed that the Raman transitions are in two-photon resonance. On the other hand the single-photon transitions shall have a large detuning $\Delta_\pm$ such that the excited states can be adiabatically eliminated. To illustrate the adiabatic elimination procedure let us consider only a single Λ system $\{|g\rangle, |e\rangle, |s\rangle\}$. Assume an optical dipole coupling $|g\rangle \leftrightarrow |e\rangle$ with coupling strength or Rabi frequency Ω_1 as well as $|s\rangle \leftrightarrow |e\rangle$ with coupling strength Ω_2. If both optical couplings are in two photon, i.e., Raman resonance, but have a common detuning Δ to the excited state, the equation of motion of the atomic wave function $|\psi(t)\rangle = c_g(t)|g\rangle + c_e(t)|e\rangle + c_s(t)|s\rangle$ reads

$$\frac{\mathrm{d}}{\mathrm{d}t}\begin{pmatrix} c_g(t) \\ c_e(t) \\ c_s(t) \end{pmatrix} = i\begin{pmatrix} 0 & \Omega_1^* & 0 \\ \Omega_1 & \Delta & \Omega_2 \\ 0 & \Omega_2^* & 0 \end{pmatrix}\begin{pmatrix} c_g(t) \\ c_e(t) \\ c_s(t) \end{pmatrix}.$$

If $|\Delta| \gg |\Omega_{1,2}|$ we can neglect the time derivative in the second line (adiabatic elimination of the excited state) and approximate $c_e(t) \approx \Omega_1 c_g(t)/\Delta + \Omega_2 c_s(t)/\Delta$. Substituting this result in the above equations yields

$$\frac{\mathrm{d}}{\mathrm{d}t}\begin{pmatrix} c_g(t) \\ c_s(t) \end{pmatrix} = i\begin{pmatrix} 0 & \dfrac{\Omega_1^*\Omega_2}{\Delta} \\ \dfrac{\Omega_1\Omega_2^*}{\Delta} & 0 \end{pmatrix}\begin{pmatrix} c_g(t) \\ c_s(t) \end{pmatrix}.$$

Since the individual optical Rabi frequencies have a time dependence $\Omega_{1,2} \sim e^{-i\omega_{1,2}t}$, the two-photon Rabi frequency $\Omega_1^*\Omega_2/\Delta$ has a slow frequency. Generalizing the above discussion to the two parallel Λ transition of Fig. 16 and replacing one of the two fields of each Λ transition by the common quantized probe field $\hat{E}$ leads to the effective Hamiltonian

$$\hat{H}_{\text{eff}} \sim \sum_j \left[\frac{\Omega_+^*\vec{d}_+}{\Delta_+}\sigma^j_{s,g}\hat{\vec{E}}^{(-)}(z_j) + \frac{\Omega_-^*\vec{d}_-}{\Delta_-}\sigma^j_{g,s}\hat{\vec{E}}^{(-)}(z_j) + \text{H.c.}\right], \quad (55)$$

which exactly corresponds to that of the spin-boson model.

IV. SUMMARY

In the present paper we have analyzed the coupling of quantum dipole oscillators to the plasmon modes of an infinite cylindrical nanowire by means of a Green's function approach taking into account wire losses. Placing a single emitter close to the surface of a cylindrical metallic wire with subwavelength radius, there is a strong interaction between the emitter and the traveling surface plasmon modes of the metal. The magnitude of the interaction becomes apparent in a substantial increase in the total spontaneous decay rate going up to several hundred times the vacuum value. When decreasing the wire radius, only the fundamental cylindrical mode survives with a rapidly increasing radial confinement, allowing for a single-mode wire and an increasingly strong emitter-plasmon interaction. We have calculated the spectrum of the plasmon modes and analyzed their broadening in the presence of metal losses ($\epsilon'' \neq 0$) for different wire radii R. For fixed ϵ'', the broadening and the associated propagation losses increase with decreasing wire radius since a growing part of the field is concentrated inside the wire. For a subwavelength nanowire the dependence of the resonance width on the wire radius turns from an $R^{-1/2}$ to an $R^{-3/2}$ behavior. We derived explicit expressions for the coupling strength of an atom to the plasmon modes and discussed its relation to nonplasmonic couplings and how it depends on the wire parameters and the atom-wire distance. For nonvanishing material losses there is an optimum emitter-wire distance for which the decay rate into the plasmons relative to the total decay rate is maximal. We also discussed the plasmon-mediated coupling between two quantum dipoles. Putting two emitters close to the wire results in Dicke subradiance and superradiance even when the separation of the emitters along the wire exceeds the vacuum wavelength by an order of magnitude. Depending on the precise distance between the emitters, the decay rate of the symmetric or the antisymmetric Dicke state is enhanced or suppressed. Similar to the one-atom case due to the finite material losses there is an optimum emitter-surface distance yielding the maximal coupling between the atoms. Also, for a given interatomic distance there exists an optimal wire radius for which the coupling between the emitters is maximal. The possibility to control the symmetric and antisymmetric decay rates allows to build two-qubit quantum gates using the setup. We proposed and analyzed a scheme for a deterministic two-qubit phase gate. The achievable gate fidelity for realistic parameters is on the order of 80%. This can be attributed to two loss mechanisms: wire absorption of plasmons and spontaneous emission into free-space radiation modes. For small values of ϵ'' the fidelity could be improved by embedding the atoms in a photonic band-gap material, suppressing the free-space spontaneous emission. Furthermore, introducing a wire ring instead of an infinite cylinder, the effect from the loss of excitation along the wire may be reduced while retaining the strong coupling. Additionally, a geometry-independent analysis shows that, asymptotically, the gate fidelity error scales as $\sqrt{\Gamma_S/\Gamma_{eg}}$, i.e., the square root of the ratio between the symmetric (subradiant) and one-atom decay rate, as $F \to 1$. Finally atoms coupled to plasmonic nanowires may also be an interesting system for the realization of interesting spin models such as the spin-boson model.

ACKNOWLEDGMENTS

David Dzsotjan acknowledges financial support by the EMALI Marie-Curie Network, by the Research Fund of the Hungarian Academy of Sciences (OTKA) under Contract No. 78112 and by the German Research Foundation (DFG) under Contract No. FL210/15-1. A.S.S. acknowledges the support of the Villum Kann Rasmussen foundation and the Danish National Science Research Foundation. The authors would like to thank P. Rabl for valuable discussions.

[1] D. E. Chang, A. S. Sørensen, P. R. Hemmer, and M. D. Lukin, Phys. Rev. Lett. **97**, 053002 (2006).
[2] D. E. Chang, A. S. Sørensen, P. R. Hemmer, and M. D. Lukin, Phys. Rev. B **76**, 035420 (2007).
[3] J. Takahara, S. Yamagishi, H. Taki, A. Morimoto, and T. Kobayashi, Opt. Lett. **22**, 475 (1997).
[4] V. V. Klimov, M. Ducloy, and V. S. Letokhov, Chem. Phys. Lett. **358**, 192 (2002).
[5] I. I. Smolyaninov, J. Elliott, A. V. Zayats, and C. C. Davis, Phys. Rev. Lett. **94**, 057401 (2005).
[6] K. Kneipp, Y. Wang, H. Kneipp, L. T. Perelman, I. Itzkan, R. R. Dasari, and M. S. Feld, Phys. Rev. Lett. **78**, 1667 (1997).
[7] S. Nie and S. R. Emory, Science **275**, 1102 (1997).
[8] S. Kühn, U. Håkanson, L. Rogobete, and V. Sandoghdar, Phys. Rev. Lett. **97**, 017402 (2006).
[9] Y. T. Chen, T. R. Nielsen, N. Gregersen, P. Lodahl, and J. Mork, Phys. Rev. B **81**, 125431 (2010).
[10] X. W. Chen, V. Sandoghar, and M. Agio, Nano Lett. **9**, 3756 (2009).
[11] D. E. Chang, A. S. Sørensen, E. A. Demler, and M. D. Lukin, Nat. Phys. **3**, 807 (2007).
[12] A. V. Akimov, A. Mukherjee, C. L. Yu, D. E. Chang, A. S. Zibrov, P. R. Hemmer, H. Park, and M. D. Lukin, Nature (London) **450**, 402 (2007).
[13] A. L. Falk, F. H. L. Koppens, C. L. Yu, K. Kang, N. D. Snapp, A. V. Akimov, M. H. Jo, M. D. Lukin, and H. Park, Nat. Phys. **5**, 475 (2009).
[14] R. Kolesov, B. Grotz, G. Balasubramanian, R. J. Stohr, A. A. L. Nicolet, P. R. Hemmer, F. Jelezko, and J. Wrachtrup, Nat. Phys. **5**, 470 (2009).
[15] F. Le Kien, S. DuttaGupta, K. P. Nayak, and K. Hakuta, Phys. Rev. A **72**, 063815 (2005).
[16] H. T. Dung, S. Y. Buhmann, L. Knöll, D. G. Welsch, S. Scheel, and J. Kästel, Phys. Rev. A **68**, 043816 (2003).
[17] L. Knöll, S. Scheel, and D.-G. Welsch, in *Coherence and Statistics of Photons and Atoms*, edited by J. Peřina (Wiley, New York, 2001).
[18] L. W. Li, M. S. Leong, T. S. Yeo, P. S. Kooi, and J. El, J. Electromagn. Waves Appl. **14**, 961 (2000).
[19] M. Fleischhauer, Phys. Rev. A **60**, 2534 (1999).
[20] J. Kästel and M. Fleischhauer, Phys. Rev. A **71**, 011804(R) (2005).
[21] J. Kästel and M. Fleischhauer, Laser Phys. **15**, 135 (2005).
[22] E. Vetsch, D. Reitz, G. Sagu, R. Schmidt, S. T. Dawkins, and A. Rauschenbeutel, arXiv:0912.1179 (unpublished).
[23] W. Schnitzler, N. M. Linke, R. Fickler, J. Meijer, F. Schmidt-Kaler, and K. Singer, Phys. Rev. Lett. **102**, 070501 (2009).
[24] I. Bloch, J. Dalibard, and W. Zwerger, Rev. Mod. Phys. **80**, 885 (2008).
[25] F. Dimer, B. Estienne, A. S. Parkins, and H. J. Carmichael, Phys. Rev. A **75**, 013804 (2007).